

Magnetic-field-sensitive charge density waves in the superconductor UTe_2

<https://doi.org/10.1038/s41586-023-06005-8>

Received: 27 July 2022

Accepted: 23 March 2023

Published online: 28 June 2023

 Check for updates

Anuva Aishwarya¹, Julian May-Mann^{1,2}, Arjun Raghavan¹, Laimei Nie^{1,2}, Marisa Romanelli¹, Sheng Ran^{3,4,5}, Shanta R. Saha³, Johnpierre Paglione^{3,6}, Nicholas P. Butch^{3,4}, Eduardo Fradkin^{1,2} & Vidya Madhavan^{1,6}✉

The intense interest in triplet superconductivity partly stems from theoretical predictions of exotic excitations such as non-Abelian Majorana modes, chiral supercurrents and half-quantum vortices^{1–4}. However, fundamentally new and unexpected states may emerge when triplet superconductivity appears in a strongly correlated system. Here we use scanning tunnelling microscopy to reveal an unusual charge-density-wave (CDW) order in the heavy-fermion triplet superconductor UTe_2 (refs. 5–8). Our high-resolution maps reveal a multi-component incommensurate CDW whose intensity gets weaker with increasing field, with the CDW eventually disappearing at the superconducting critical field H_{c2} . To understand the phenomenology of this unusual CDW, we construct a Ginzburg–Landau theory for a uniform triplet superconductor coexisting with three triplet pair-density-wave states. This theory gives rise to daughter CDWs that would be sensitive to magnetic field owing to their origin in a pair-density-wave state and provides a possible explanation for our data. Our discovery of a CDW state that is sensitive to magnetic fields and strongly intertwined with superconductivity provides important information for understanding the order parameters of UTe_2 .

In the ongoing search for new phases of matter, the heavy-fermion superconductor uranium ditelluride (UTe_2), which combines strong correlations and triplet superconductivity^{5–8} with possible non-trivial topology^{9–11}, is an extremely promising system. UTe_2 is paramagnetic, exhibiting no magnetic ordering down to the lowest temperatures¹², and superconducts below the critical temperature (T_c) of about 2 K (refs. 5,8). The unusually high upper critical field (H_{c2})⁵, multiple field-reentrant superconducting phases⁷, minimal change in the Knight shift^{5,12} and exceptionally large Sommerfeld coefficient below T_c (ref. 5) all provide strong evidence in support of unconventional triplet superconductivity. Recent measurements of a non-zero polar Kerr effect below T_c (ref. 10) show that the superconducting state may have broken time-reversal symmetry. Theoretical studies suggest that UTe_2 might be a topologically non-trivial Weyl superconductor^{11,13,14} and harbour a chiral triplet state with Majorana arcs^{15,16}. These phenomena combined with indications of non-trivial topology make UTe_2 an exciting and unique platform for the realization of fundamentally new states.

In this work, we use scanning tunnelling microscopy and scanning tunnelling spectroscopy to study single crystals of UTe_2 below T_c . UTe_2 crystallizes into a body-centred orthorhombic structure with two uranium atoms per unit cell¹⁷. The unit cell consists of bi-trigonal prisms of U and Te in which a U–U dimer is surrounded by two inequivalent Te atoms (based on U–Te bond lengths) labelled Te1 and Te2 in Fig. 1a (dark and light blue colours). The chains of bi-trigonal prisms run parallel to the *a* direction and are offset by *c*/2 in the *c* direction (Fig. 1b), in which

c is the height of the unit cell. The lattice may also be visualized as slabs of bi-trigonal prisms oriented along the (011) direction (Fig. 1b). The UTe_2 samples in this study were cleaved at temperatures of about 90 K and immediately inserted into the head of the scanning tunnelling microscope (see Methods and Extended Data Fig. 1 for details). Previous studies⁹ have shown that (011) is the easy-cleave plane and the atoms readily visible in the topography are the Te1 and Te2 atoms, which appear as chains (Fig. 1c,d). A fast Fourier transform (FFT) of the topography is shown in Fig. 1g, in which the Te Bragg peaks are shown by cyan dashed arrows. We denote the Te Bragg peaks as $q_{1,2}^{\text{Te}} = (\pm q_{0x}, q_{0y})$, in which q_{0x} and q_{0y} represent coordinates in the *x* and *y* directions in the FFT as labelled. Note that the *x* and *y* directions used here are for ease of notation and do not indicate the crystallographic directions. To complete the picture, we identify the (011) projection plane of the three-dimensional orthorhombic Brillouin zone (BZ) in momentum space as shown in Fig. 1e. Constructing the BZ for the surface from the primitive lattice vectors gives rise to an elongated, hexagonal BZ as shown in Fig. 1g. The centre of this BZ is labelled as S and the vertices are labelled as L_1 , L_2 and W by convention¹⁸.

Incommensurate CDWs in the superconducting state

As is evident from Fig. 1g, apart from the Te Bragg peaks, there are three additional peaks (outlined by two squares and a triangle), near the L_1 , L_2 and W points of the BZ in the FFT. To understand the origin of these

¹Department of Physics and Materials Research Laboratory, University of Illinois at Urbana-Champaign, Urbana, IL, USA. ²Institute for Condensed Matter Theory, University of Illinois, Urbana, IL, USA. ³Maryland Quantum Materials Center, Department of Physics, University of Maryland, College Park, MD, USA. ⁴NIST Center for Neutron Research, National Institute of Standards and Technology, Gaithersburg, MD, USA. ⁵Department of Physics, Washington University in St. Louis, St Louis, MO, USA. ⁶Canadian Institute for Advanced Research, Toronto, Ontario, Canada.

✉e-mail: vm1@illinois.edu

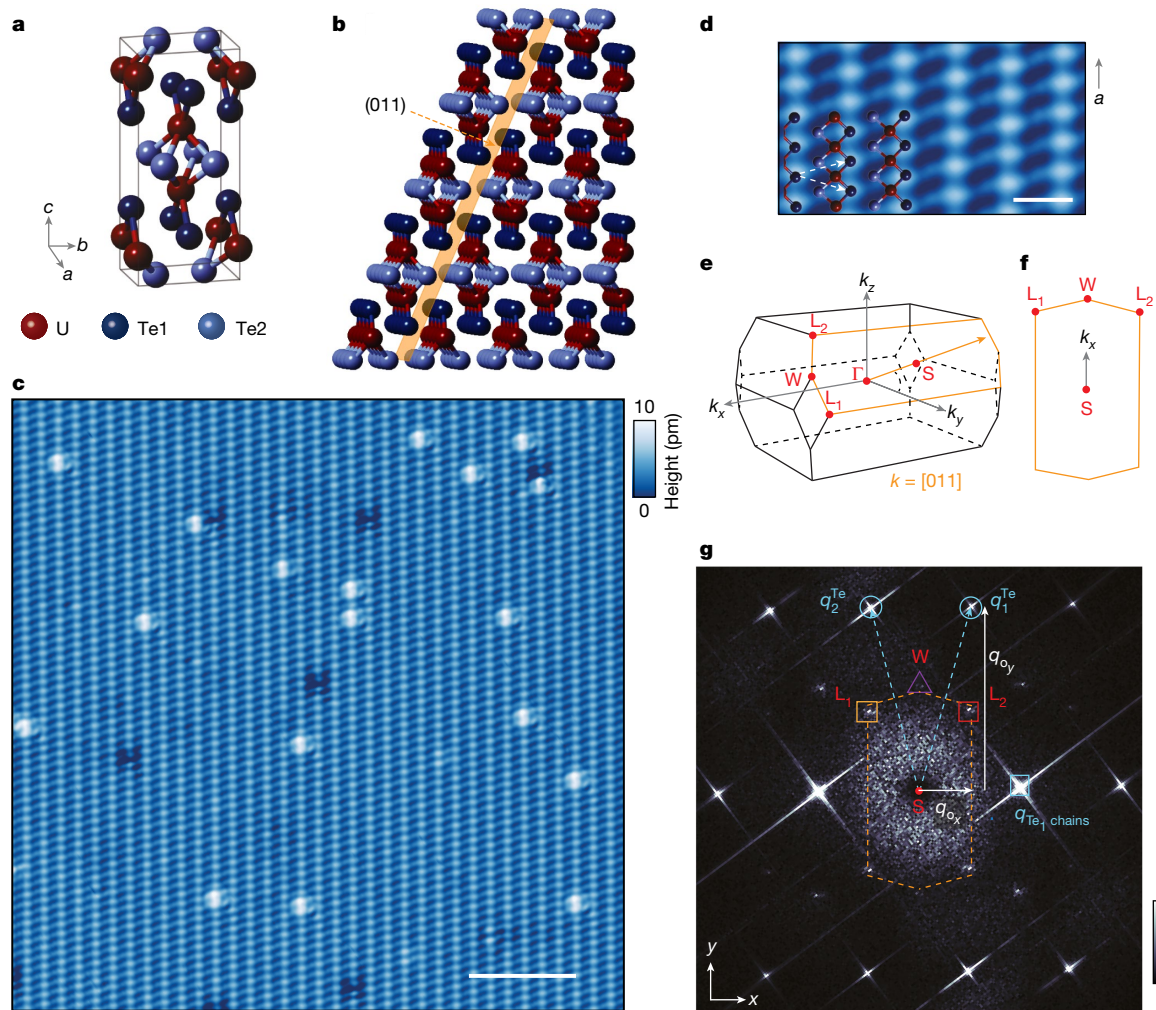


Fig. 1 | Crystal structure and the (011) cleave surface in real space and Fourier space. **a**, Unit cell of UTe_2 , consisting of U–U dimers and two inequivalent Te sites labelled as Te1 and Te2 depicted here by two different shades of blue. **b**, (011) easy-cleave plane indicated by the yellow lattice plane. Cleaving along (011) exposes a plane of Te1 and Te2 atoms, with the U directly underneath. **c**, A large area, atomically resolved topography obtained at $T = 300$ mK showing the Te1 and Te2 atoms ($V = -60$ mV, $I = 200$ pA) with the Te1 chains being more prominent. Scale bar, 50 Å. **d**, A high-resolution, zoomed-in view of the atomic lattice ($V = -60$ mV, $I = 200$ pA). A schematic of the lattice has been overlaid on top to show the relative positions of the atoms. Scale bar, 10 Å. The dashed arrows indicate the primitive lattice vectors. **e**, Schematic of the

first BZ of an orthorhombic crystal with k_x , k_y and k_z directions indicated by grey arrows. The relevant points in the BZ are labelled in red. The orange hexagon is the (011) plane in reciprocal space. **f**, Schematic of the BZ with the momentum space points L_1 , L_2 and W labelled in red. **g**, Fourier transform of the topography shown in **c**. The Bragg peak indicated by the cyan circle comes from the Te1–Te1 spacing (in the y direction) along the chains (which is the same as the Te2–Te2 and U–U distances along the chain). The Bragg peak within the cyan square comes from the inter-chain spacing (in the x direction). The reciprocal lattice vectors are shown by the dashed arrows. The schematic of the BZ is overlaid on the FFT. The orange and red squares and the purple triangle indicate the positions where the CDW peaks are observed. H, high; L, low.

extra peaks, we carry out spectroscopic imaging (that is, we obtain the differential tunnelling conductance $\frac{dI}{dV}(r, E)$ maps as a function of energy (E)). A $\frac{dI}{dV}(r, E)$ map is directly proportional to the local density of states (LDOS) and can provide information about the band structure through quasiparticle interference as well as Fermi surface instabilities such as CDWs. In addition to the atomic corrugation of the Te lattice, the LDOS maps (Fig. 2a–c and Extended Data Fig. 2) show modulations both above and below the Fermi energy (E_F) that are distinct from the lattice. This additional modulation is also captured in the FFTs shown in Fig. 2d–f (full dataset in Extended Data Fig. 3) and gives rise to the same additional peak structure seen in the FFT of the topography shown in Fig. 1g.

To distinguish between signals from quasiparticle interference and CDWs, we study the energy dependence of the q vectors associated with the peaks in the FFT. To do this, we obtain linecuts of the FFTs of the LDOS maps in the three important momentum space directions, S– L_1 , S– L_2 and S– W (henceforth labelled as line 1, 2 and 3, respectively)

and plot this as a function of energy. This information is presented as an intensity map in Fig. 2g–i. Contrary to energy-dispersive features such as quasiparticle interference, we find that the magnitude of the three q vectors shows no energy dependence. This indicates that the observed modulations arise from a multi-component CDW order in this material. We have verified the existence of these CDWs across 11 different samples and tips from three different growth batches. We label the CDWs that are shown by the orange square, red square and purple triangle as q_i^{CDW} , in which $i = 1, 2, 3$, respectively. The CDW q vectors are $q_1^{\text{CDW}} = (-q_{0x}, 0.43q_{0y})$, $q_2^{\text{CDW}} = (q_{0x}, 0.43q_{0y})$ and $q_3^{\text{CDW}} = (0, 0.57q_{0y})$, in which q_{0x} and q_{0y} are the coordinates associated with $q_{1,2}^{\text{Te}}$. We note that all three CDWs are incommensurate with the underlying lattice. q_1^{CDW} and q_2^{CDW} are related by mirror symmetry and q_3^{CDW} can be connected to q_1^{CDW} and q_2^{CDW} by a lattice vector. These may therefore in principle correspond to a single CDW order, but for the purposes of this paper (the reason will be clear when we look at the field dependence), we treat them as independent order parameters.

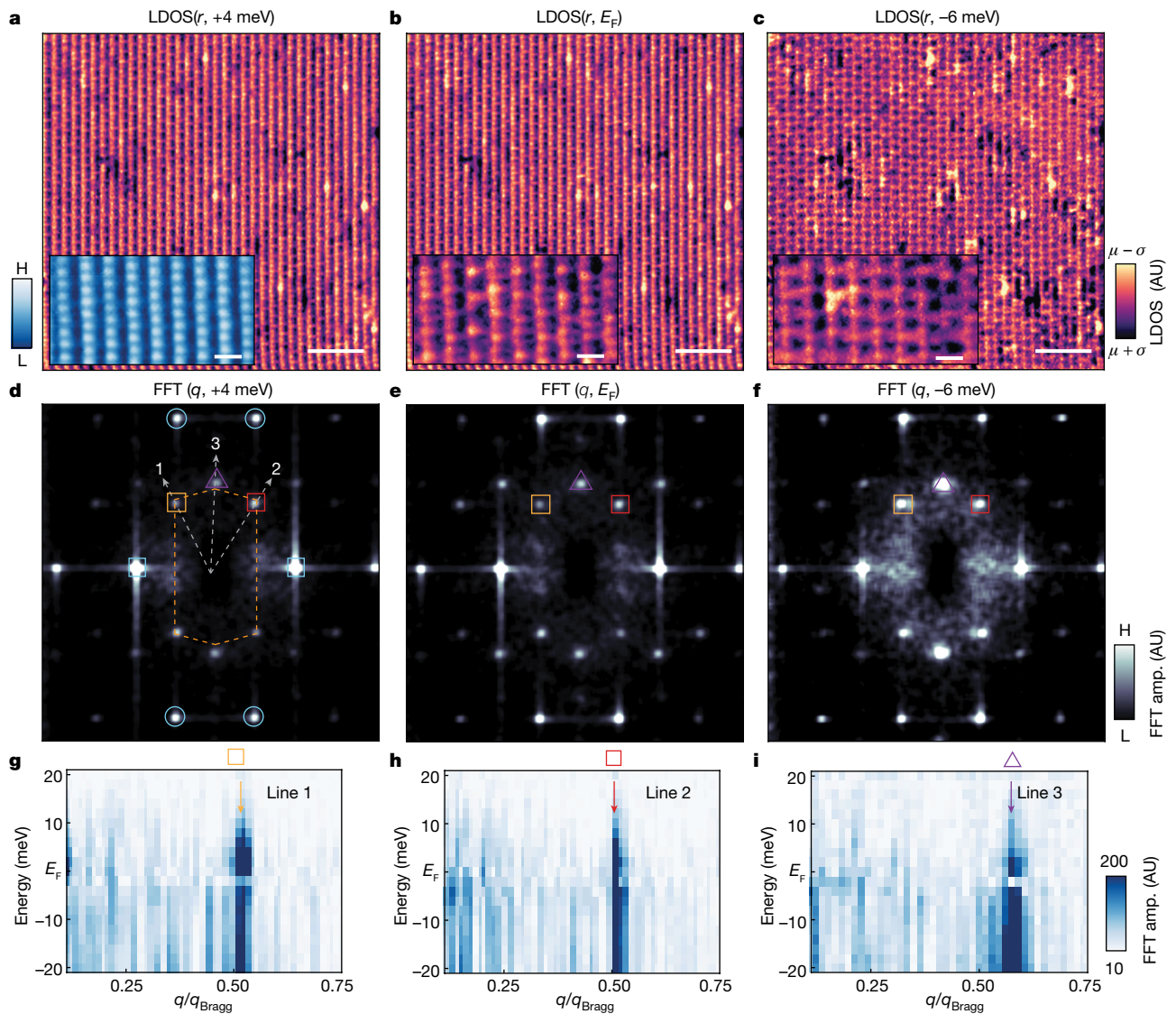


Fig. 2 | Spectroscopic imaging of the three distinct CDW orders. **a–c**, LDOS maps obtained on a $30 \text{ nm} \times 30 \text{ nm}$ area at various energies (see Extended Data Figs. 2 and 3 for the complete set). The energies are shown above each map. Scale bars, 50 \AA ($T = 300 \text{ mK}$, tunnelling setpoint: $V = 50 \text{ mV}$, $I = 250 \text{ pA}$). Insets of **b, c** show atomically resolved LDOS maps at similar energies. The corresponding topography is shown as an inset to **a**. Scale bars, 10 \AA . AU, arbitrary units. **d–f**, FFTs of the LDOS maps shown in **a–c**. The cyan circles and squares indicate the lattice Bragg peaks. The orange dashed hexagon indicates the BZ. The orange and red squares and the purple triangle indicate the

positions where the extra CDW peaks are observed. The momentum points L_1 , L_2 and W (shown in Fig. 1) are close to the orange square, red square and purple triangle, respectively (that is, the q_i^{CDW} points are very close to the BZ vertices). **g–i**, Linecuts in Fourier space plotted as an intensity map along the three directions shown by the grey arrows in **d**. The positions of the peaks in the FFT (that is, the q vectors) do not change with energy, consistent with a CDW. The magnitudes of q_1^{CDW} and q_2^{CDW} are close to half of q_{Te} (that is, $2a_{Te-Te}$ or $2a_{U-U}$ in real space). The magnitude of q_3^{CDW} is about $0.55q_{Te}$ (about $1.78a_{Te-Te}$ or about $1.78a_{U-U}$ in real space).

The observation of a CDW in a superconductor immediately leads to the question of its relationship with superconductivity. In most instances when a CDW is found in the superconducting phase, it is an independent order parameter, which could coexist and/or compete with superconductivity¹⁹. There is however a more interesting scenario in which a CDW is a direct consequence of a periodically modulated superconducting order parameter or a pair-density-wave (PDW) phase^{20–25}. A PDW is a new phase of matter for which the superconducting order parameter shows periodic spatial oscillations. A unidirectional PDW state can coexist with a uniform superconductor. In this scenario, a PDW with wavevector \mathbf{Q} is expected to generate a CDW at both \mathbf{Q} and $2\mathbf{Q}$ (ref. 22). In a scenario with three CDWs, we would invoke PDWs with three primary ordering wavevectors \mathbf{Q}_i ($i = 1, 2, 3$), which coexist with the uniform superconducting state. The associated CDWs should then show the same primary ordering wavevectors as

well as their linear combinations ('higher harmonics') playing the role of the above-mentioned $2\mathbf{Q}$ component. PDWs have been proposed to exist in superconductors with an in-plane field^{26,27}, but zero-field PDWs require strong interactions. Experimental data showing evidence for this exotic state have been limited to cuprates^{28–34} and more recently to kagome superconductors^{35–39}.

Magnetic field response of the CDWs

To investigate the relationship between the CDWs and superconductivity, we study the effect of magnetic fields on the CDW. As the magnetic field is perpendicular to the (011) cleave plane and to the a axis, it makes an angle of 23.7° with the b axis (Fig. 3a). Extremely high magnetic fields (about 40 T) oriented along this direction give rise to the mysterious Lazarus superconducting phase or the field-polarized superconducting

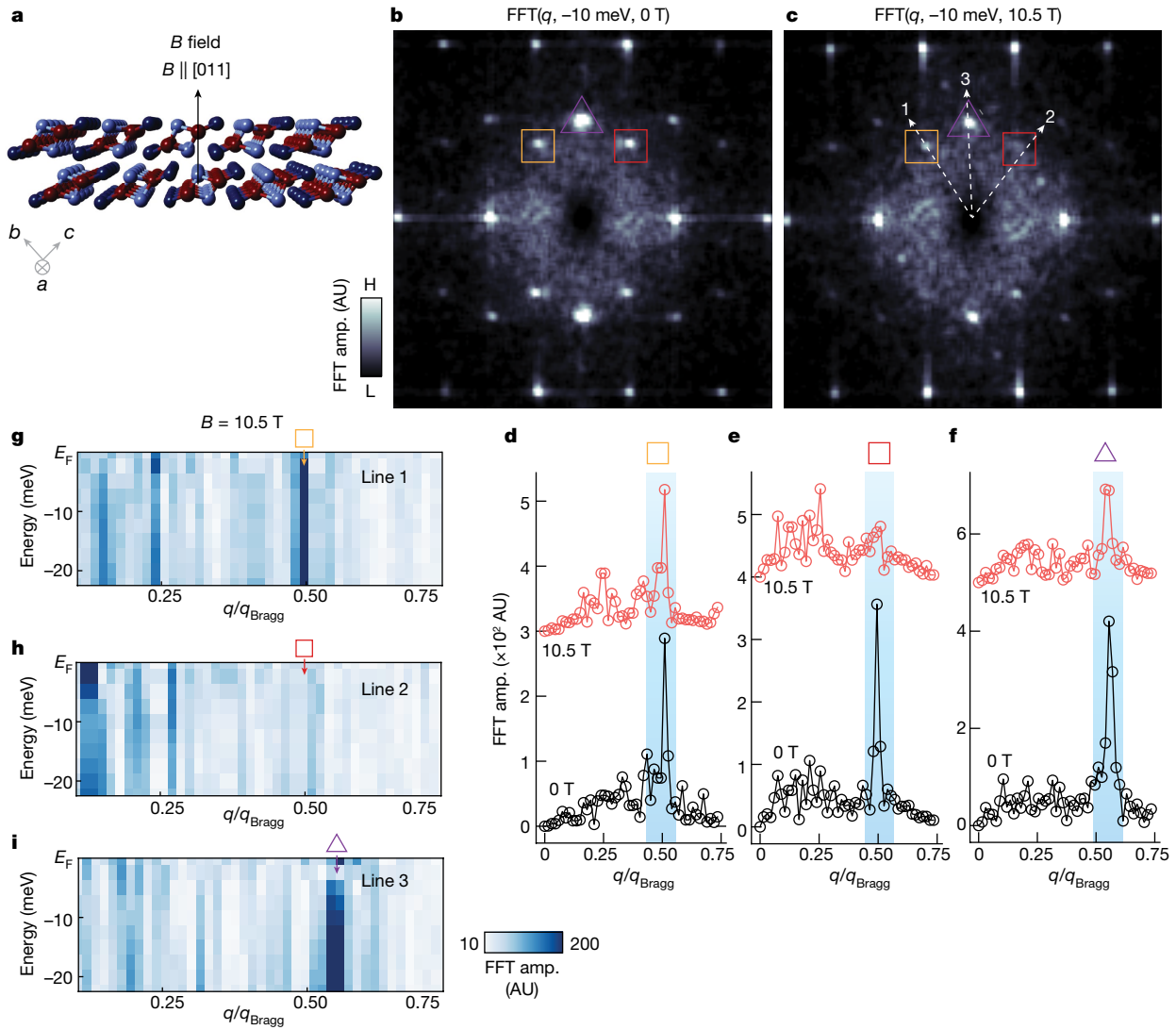


Fig. 3 | Suppression and mirror-symmetry breaking of the CDWs in a perpendicular magnetic field. **a**, Schematic showing the direction of the applied magnetic field with respect to the (011) plane. **b, c**, FFTs of LDOS maps at 0 T and 10.5 T with the CDWs marked. The data were obtained on the same area as the 0 T data shown in Fig. 2 and obtained at -10 meV ($T = 300$ mK, tunnelling setpoint: $V = 50$ mV, $I = 250$ pA). The colour scale has been kept identical for **b, c**. **d–f**, Linecuts of the Fourier transforms of the LDOS maps at a single energy (-10 meV), along the three different CDW directions and of (indicated by the dashed arrows in **c**) for the FFT at 0 T and 10.5 T, respectively.

phase⁷. Remarkably, at our much smaller fields, we see a peculiar response of the CDWs to the magnetic field. Figure 3b,c shows FFTs at 0 T and 10.5 T. The data in Fig. 3 (at 10.5 T) were obtained on the same sample with the same tip, with identical setpoint and tunnel current as the data in Fig. 2 (that is, at 0 T). First, we find that all three CDWs are substantially suppressed in field. This can be seen by comparing the FFT at 10.5 T with the FFT at 0 T, as illustrated by linecuts obtained along the three directions (Fig. 3d–f). We also find that the CDWs in field are not equally suppressed (that is, q_2^{CDW} is suppressed much more strongly than q_1^{CDW}), breaking mirror symmetry. The mirror-symmetry breaking is not confined to just one energy, as shown by the energy-dependent plot of the CDW intensity (Fig. 3g–i and Extended Data Figs. 5–7). This phenomenology was confirmed with two separate tip and sample combinations (Extended Data Fig. 8).

Notably, the suppression of the CDW with field is further enhanced when the magnetic field is tilted slightly with respect to the [011]

The CDWs are marked by the orange and red squares and purple triangle. Although all of the CDW peaks are substantially suppressed, the CDW along line 2 as shown in **e** shows a much stronger suppression in comparison to **d**. This reveals a putative breaking of the mirror symmetry in the presence of a magnetic field. **g–i**, Linecuts of FFTs at 10.5 T at different energies along the three directions indicated by the dashed arrows in **c**, plotted as an intensity map. One can visually see that the Fourier amplitude at in **h** is highly suppressed compared to the 0 T data in Fig. 2h.

direction. We can generate such a tilt in the sample while mounting the sample on the sample holder. Although these angles at present cannot be tuned controllably, they can provide valuable insights for a crystal such as UTe_2 whose superconducting properties are highly sensitive to magnetic field orientation⁷. Figure 4 shows magnetic-field-dependent measurements obtained on one such fortuitous sample with a 11° tilt. Figure 4b–d shows a series of FFTs of topographies obtained at selected magnetic fields, and Fig. 4f–h shows FFT linecuts obtained along the three different momentum space directions. The intensities of the CDW peaks are once again suppressed with magnetic field, with the CDWs eventually disappearing at around 10 T. This is captured in Fig. 4e, which plots the intensity of the different CDW peaks normalized to the Te Bragg peak as a function of field. We find that the CDW order parameter is concomitantly suppressed with superconductivity. This phenomenology was confirmed with other tip–sample combinations (see Extended Data Fig. 10). The complete disappearance of the CDW at

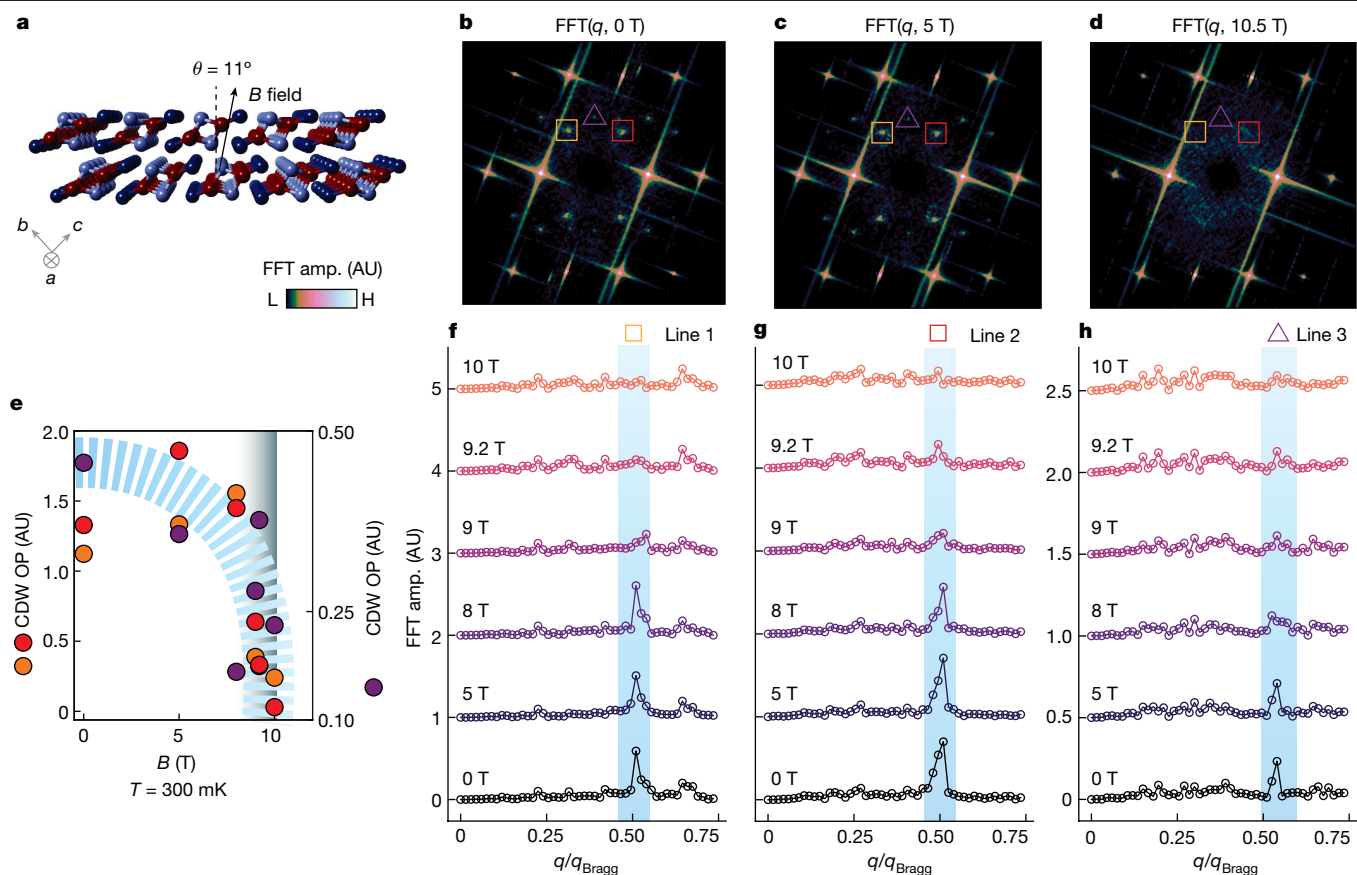


Fig. 4 | Disappearance of the CDWs above H_{c2} for magnetic field tilted at 11° to the [011] direction. **a**, Schematic of the direction of the applied magnetic field with respect to the (011) plane. The magnetic field is tilted 11° with respect to the [011] direction. **b–d**, FFTs obtained at 0 T (**b**), 5 T (**c**) and 10.5 T (**d**) on the same area with identical settings at $T = 300$ mK ($V = -40$ mV, $I = 120$ pA). The CDWs are marked by the orange and red squares and purple triangle. The colour scale has been kept constant for **b–d**. **e**, Plot of the strength of the CDW order parameter (OP; Fourier amplitude of the CDW peak normalized with respect to q_{T_c}) as a

function of magnetic field. The markers are colour-coded to represent the respective CDWs. Blue dashed region is a guide to the eye. The H_{c2} is indicated by the grey region. **f–h**, Fourier transform linecuts obtained along three different directions of the CDWs as a function of magnetic field, showing clear suppression of the peak amplitudes above 9 T. The y-axis scale for **f** and that for **g** are identical. The linecuts for **h** were obtained from FFTs of topographies at positive energies (refer to Extended Data Fig. 9) for which q_3^{CDW} has a stronger signal. FFTs at positive and negative energies both show the same behaviour.

the 11° -tilted field is consistent with the lower H_{c2} value when the field is applied in this direction⁷.

Ginzburg–Landau theory

Conventionally, a CDW order is a periodic modulation of the local charge density, and as such is not expected to couple substantially to an external magnetic field except in unconventional cases such as in the kagome system, for which there are preliminary indications of an exotic chiral CDW state (presumably carrying local orbital currents) that reverses chirality in field^{36,39–41}. This leaves us with two unexplained phenomena: the suppression of the CDWs with magnetic field; and the asymmetric behaviour of the two mirror-symmetry-related CDWs with field. To provide a possible explanation for our data, we construct a Ginzburg–Landau theory that considers a triplet superconductor suggested by the symmetries of UTe_2 . We construct a model for multi-component triplet PDW order that coexists with a uniform triplet superconductor order. In this scenario, the multi-component CDW occurs as a ‘daughter’ order of the superconducting orders:

$$\rho_{q_i^{\text{CDW}}} \propto \Delta_{+q_i^{\text{CDW}}} \cdot \Delta_0^* + \Delta_0 \cdot \Delta_{-q_i^{\text{CDW}}}^* + \text{h. c.},$$

in which $\Delta_{\pm q_i^{\text{CDW}}}$ is the PDW order parameter with wavevector $\pm q_i^{\text{CDW}}$, and Δ_0 is the uniform triplet superconductivity order parameter.

A Ginzburg–Landau theory analysis of these orders leads to the following conclusions: above the upper critical field of the superconducting orders, the PDW and uniform superconducting orders are suppressed, as are the daughter CDWs; owing to the triplet nature of the superconducting order parameter, the critical magnetic field is direction dependent; and as $\Delta_{+q_1^{\text{CDW}}}$ and $\Delta_{+q_2^{\text{CDW}}}$ are related by mirror symmetry, one of the two corresponding mirror-related CDWs may be more suppressed than the other when mirror symmetry is broken by an external magnetic field. A coexisting triplet PDW order is therefore a possible explanation for the unusual magnetic field response of the CDWs as seen in our experiments.

Discussion

It is important to consider whether there might be other explanations for our data. There are in fact very few alternative explanations for a CDW that is sensitive to magnetic fields. Two other possibilities are that the CDW is a daughter order of a spin density wave, or that the CDW itself has a finite angular momentum, similar to what has been observed in kagome superconductors. Although both of these scenarios might explain the dependence of the CDW on a magnetic field, they each have limitations. First, no static magnetic order has been observed in UTe_2 by other experimental probes^{5,17,42}, which makes the spin density wave explanation unlikely. Second, the fact that the critical field for the CDW

suppression is close to the critical field of the superconductor is difficult to explain with either the spin density wave or the finite angular momentum CDW possibility. In a nutshell, although our data are most consistent with the existence of a triplet PDW state in UTe_2 , additional theory as well as experimental tests are important to unequivocally establish this scenario. We note here that as scanning tunnelling microscopy probes the surface, the natural question is whether these orders are also observed in the bulk. This calls for bulk measurements such as low-temperature X-ray scattering measurements.

There are two further points to mention. Our preliminary temperature-dependent measurements indicate that the CDW (as seen in the FFT) survives to 4 K and disappears somewhere between 4 K and 10 K (Extended Data Fig. 11). This is not inconsistent with the PDW scenario, as the PDW can melt to a CDW phase, which can survive at higher temperatures. A more detailed discussion of this question is presented in the Methods. The other question concerns the identification of the observed peaks with the primary ordering peaks (**1Q**) or their linear combinations (**2Q**). The peaks we observe may represent the primary **1Q** peaks as we do not see any peaks at smaller q vectors in the FFT. Consistent with this, all linear combinations of the primary peaks and Bragg peaks are also observed in our data (see Extended Data Fig. 4).

To conclude, we report the observation of multi-component, incommensurate CDW order coexisting with superconductivity in UTe_2 . Strikingly, we observe that the CDWs are strongly affected by an external magnetic field and vanish at the H_{c2} of the superconducting order. This last observation clearly implies that the CDW and superconducting order parameters are not merely coexisting but are in fact strongly coupled. This, combined with the established presence of a uniform triplet order, may indicate that the superconducting state of UTe_2 has a triplet PDW component, which necessitates strong interactions.

Online content

Any methods, additional references, Nature Portfolio reporting summaries, source data, extended data, supplementary information, acknowledgements, peer review information; details of author contributions and competing interests; and statements of data and code availability are available at <https://doi.org/10.1038/s41586-023-06005-8>.

- Sigrist, M. & Ueda, K. Phenomenological theory of unconventional superconductivity. *Rev. Mod. Phys.* **63**, 239 (1991).
- Reed, N. & Green, D. Paired states of fermions in two dimensions with breaking of parity and time-reversal symmetries and the fractional quantum Hall effect. *Phys. Rev. B* **61**, 10267 (2000).
- Kitaev, A. Y. Unpaired Majorana fermions in quantum wires. *Phys.-Usp.* **44**, 131 (2001).
- Ivanov, D. A. Non-Abelian statistics of half-quantum vortices in p-wave superconductors. *Phys. Rev. Lett.* **86**, 268 (2001).
- Ran, S. et al. Nearly ferromagnetic spin-triplet superconductivity. *Science* **365**, 684–687 (2019).
- Aoki, D. et al. Unconventional superconductivity in heavy fermion UTe_2 . *J. Phys. Soc. Jpn* **88**, 043702 (2019).
- Ran, S. et al. Extreme magnetic field-boosted superconductivity. *Nat. Phys.* **15**, 1250–1254 (2019).
- Aoki, D. et al. Unconventional superconductivity in UTe_2 . *J. Phys. Condens. Matter* **34**, 243002 (2022).
- Jiao, L. et al. Chiral superconductivity in heavy-fermion metal UTe_2 . *Nature* **579**, 523–527 (2020).
- Hayes, I. M. et al. Multicomponent superconducting order parameter in UTe_2 . *Science* **373**, 797–801 (2021).
- Shishidou, T., Suh, H. G., Brydon, P. M. R., Weinert, M. & Agterberg, D. Topological band and superconductivity in UTe_2 . *Phys. Rev. B* **103**, 104504 (2021).

- Nakamine, G. et al. Superconducting properties of heavy fermion UTe_2 revealed by ^{125}Te -nuclear magnetic resonance. *J. Phys. Soc. Jpn* **88**, 113703 (2019).
- Metz, T. et al. Point-node gap structure of the spin-triplet superconductor UTe_2 . *Phys. Rev. B* **100**, 220504(R) (2019).
- Kittaka, S. et al. Orientation of point nodes and nonunitary triplet pairing tuned by the easy-axis magnetization in UTe_2 . *Phys. Rev. Res.* **2**, 032014(R) (2020).
- Bae, S. et al. Anomalous normal fluid response in a chiral superconductor UTe_2 . *Nat. Commun.* **12**, 2644 (2021).
- Yu, Y., Madhavan, V. & Raghu, S. Majorana fermion arcs and the local density of states of UTe_2 . *Phys. Rev. B* **105**, 174520 (2022).
- Hutanu, V. et al. Low temperature crystal structure of the unconventional spin-triplet superconductor UTe_2 from single-crystal neutron diffraction. *Acta Cryst.* **B76**, 137–143 (2020).
- Setyawan, W. & Curtarolo, S. High-throughput electronic band structure calculations: challenges and tools. *Comput. Mater. Sci.* **49**, 299–312 (2010).
- Frackin, E., Kivelson, S. A. & Tranquada, J. M. Colloquium: Theory of intertwined orders in high temperature superconductors. *Rev. Mod. Phys.* **87**, 457 (2015).
- Himeda, A., Kato, T. & Ogata, M. Stripe states with spatially oscillating d-wave superconductivity in the two-dimensional t–t′–J model. *Phys. Rev. Lett.* **88**, 117001 (2002).
- Berg, E. et al. Dynamical layer decoupling in a stripe-ordered high- T_c superconductor. *Phys. Rev. Lett.* **99**, 127003 (2007).
- Berg, E., Frackin, E. & Kivelson, S. A. Theory of the striped superconductor. *Phys. Rev. B* **79**, 064515 (2009).
- Wang, Y., Agterberg, D. F. & Chubukov, A. Coexistence of charge-density-wave and pair-density-wave orders in underdoped cuprates. *Phys. Rev. Lett.* **114**, 197001 (2015).
- Dai, Z., Zhang, Y.-H., Senthil, T. & Lee, P. A. Pair-density waves, charge-density waves, and vortices in high- T_c cuprates. *Phys. Rev. B* **97**, 174511 (2018).
- Agterberg, D. F. et al. The physics of pair-density waves: cuprate superconductors and beyond. *Annu. Rev. Condens. Matter Phys.* **11**, 231–270 (2020).
- Fulde, P. & Ferrell, R. A. Superconductivity in a strong spin-exchange field. *Phys. Rev.* **135**, A550–A563 (1964).
- Larkin, A. I. & Ovchinnikov, Y. I. Inhomogeneous state of superconductors. *Sov. Phys. JETP* **20**, 762–769 (1965).
- Hanaguri, T. et al. A ‘checkerboard’ electronic crystal state in lightly hole-doped $\text{Ca}_{2-x}\text{Na}_x\text{CuO}_2\text{Cl}_2$. *Nature* **430**, 1001–1005 (2004).
- McElroy, K. et al. Coincidence of checkerboard charge order and antinodal state decoherence in strongly underdoped superconducting $\text{Bi}_2\text{Sr}_2\text{CaCu}_2\text{O}_{8+\delta}$. *Phys. Rev. Lett.* **94**, 197005 (2005).
- Kohsaka, Y. et al. An intrinsic bond-centered electronic glass with unidirectional domains in underdoped cuprates. *Science* **315**, 1380–1385 (2007).
- Mesaros, A. et al. Commensurate $4a_0$ -period charge density modulations throughout the $\text{Bi}_2\text{Sr}_2\text{CaCu}_2\text{O}_{8+x}$ pseudogap regime. *Proc. Natl Acad. Sci. USA* **113**, 12661–12666 (2016).
- Hamidian, M. et al. Detection of a Cooper-pair density wave in $\text{Bi}_2\text{Sr}_2\text{CaCu}_2\text{O}_{8+x}$. *Nature* **532**, 343–347 (2016).
- Ruan, W. et al. Visualization of the periodic modulation of Cooper pairing in a cuprate superconductor. *Nat. Phys.* **14**, 1178–1182 (2018).
- Edkins, S. D. et al. Magnetic field–induced pair density wave state in the cuprate vortex halo. *Science* **364**, 976–980 (2019).
- Ortiz, B. R. et al. New kagome prototype materials: discovery of KV_3Sb_5 , RbV_3Sb_5 , and CsV_3Sb_5 . *Phys. Rev. Mater.* **3**, 094407 (2019).
- Jiang, Y. X. et al. Unconventional chiral charge order in kagome superconductor KV_3Sb_5 . *Nat. Mater.* **20**, 1353–1357 (2021).
- Zhao, H. et al. Cascade of correlated electron states in the kagome superconductor CsV_3Sb_5 . *Nature* **599**, 216–221 (2021).
- Chen, H. et al. Roton pair density wave in a strong-coupling Kagome superconductor. *Nature* **599**, 222–228 (2021).
- Neupert, T. et al. Charge order and superconductivity in kagome materials. *Nat. Phys.* **18**, 137–143 (2022).
- Mielke, C. et al. Time-reversal symmetry-breaking charge order in a kagome superconductor. *Nature* **602**, 245–250 (2022).
- Nie, L. et al. Charge-density-wave-driven electronic nematicity in a kagome superconductor. *Nature* **604**, 59–64 (2022).
- Duan, C. et al. Incommensurate spin fluctuations in the spin-triplet superconductor candidate UTe_2 . *Phys. Rev. Lett.* **125**, 237003 (2020).

Publisher’s note Springer Nature remains neutral with regard to jurisdictional claims in published maps and institutional affiliations.

Springer Nature or its licensor (e.g. a society or other partner) holds exclusive rights to this article under a publishing agreement with the author(s) or other rightsholder(s); author self-archiving of the accepted manuscript version of this article is solely governed by the terms of such publishing agreement and applicable law.

© The Author(s), under exclusive licence to Springer Nature Limited 2023

Scanning tunnelling microscopy experiments

Single crystals of UTe_2 were used. The growth and characterization are mentioned in detail elsewhere⁵. The crystal orientation was determined by Laue diffraction (Extended Data Fig. 1). Samples were cleaved in situ at about 90 K and in an ultrahigh-vacuum chamber. After cleaving, the samples were directly transferred to the scanning tunnelling microscope (STM) head. STM measurements were carried out using a Unisoku STM at an instrument temperature of 300 mK (unless otherwise specified) using chemically etched and annealed tungsten tips. The temperature values reported were measured at the ^3He pot; the actual sample temperature could be slightly higher. dI/dV spectra were collected using a standard lock-in technique at a frequency of 913 Hz.

Ginzburg–Landau description of the triplet PDWs

In this section we consider a Ginzburg–Landau description of triplet PDWs coexisting with a uniform triplet superconductor in a material with the same symmetries as UTe_2 . Here we shall consider both the case in which the PDW and CDW are bulk orders and the case in which they are surface orders. Our Ginzburg–Landau-based analysis applies equally well to both situations. In both cases, our theory predicts the existence of ‘daughter’ CDWs that are suppressed in an external magnetic field.

The triplet PDW

Before considering the full Ginzburg–Landau theory, it will be useful to give an overview of the triplet PDW state. In real space, we expand the local triplet Cooper pair amplitude as

$$\langle c_{\sigma}(r)c_{\sigma'}(r') \rangle = i[\tau_y \tau]_{\sigma\sigma'} \cdot [\Delta_0(r-r') + \sum_Q \Delta_Q(r-r')e^{iQ \cdot (r+r')/2}], \quad (1)$$

in which τ_i (with $i = x, y, z$) are the three 2×2 Pauli matrices, r and r' label the coordinates of the two electrons that form the Cooper pair, and the possible ordering wavevectors (and their harmonics) are given by Q . Here Δ_0 is the uniform triplet superconductor, and Δ_Q is the triplet PDW with wavevector Q . Equation (1) is applicable to both two-dimensional and three-dimensional systems. In the context of UTe_2 , Δ_0 and Δ_Q describe surface orders if r, r' and Q label positions and momentum on the surface of UTe_2 . Similarly, Δ_0 and Δ_Q correspond to bulk orders if r, r' and Q label bulk positions and momentum.

Owing to the fermion anti-commutation relationships, Δ_0 and Δ_Q must be odd functions of $r - r'$. In momentum space, the above equation becomes

$$\begin{aligned} \langle c_{\sigma}(q/2+k)c_{\sigma'}(q/2-k) \rangle \\ = i[\tau_y \tau]_{\sigma\sigma'} \cdot [\Delta_0(k)\delta^3(q) + \sum_Q \Delta_Q(k)\delta^3(q-Q)], \end{aligned} \quad (2)$$

in which k is the relative momentum of the two electrons, q is the total momentum of the Cooper pairs, and δ is the Dirac delta function. The vectors, Δ_0 and Δ_Q , are both odd functions of k . In the limit in which $Q \rightarrow 0$, Δ_Q is equivalent to the uniform triplet superconductor Δ_0 . The PDW state has the same periodic modulation of a Larkin–Ovchinnikov superconducting state²⁷ but in the absence of an external magnetic field (that is, without explicit breaking of time reversal invariance), and the period of the PDW is thus not tuned by an external magnetic field (for a review see ref. 25).

In a real material, Δ_0 and Δ_Q should form parity-odd irreducible representations (irreps) of the crystal space group. If we take Δ_0 and Δ_Q to be bulk orders of UTe_2 , then they should form irreps of D_{2h} (the space group of UTe_2). D_{2h} is characterized by three mirror symmetries, M_x, M_y and M_z (it is also possible to equivalently characterize D_{2h} in terms of three C_2 rotations). There are four parity-odd irreps of D_{2h} (ref. 43), which are referred to as A_u, B_{1u}, B_{2u} and B_{3u} . Their transformation properties of the triplet PDW, Δ_Q , under M_x are

$$\begin{aligned} M_x: \Delta_Q &\rightarrow \Delta_{M_x Q} \text{ for } \Delta_Q \in B_{1u}, B_{2u}, \\ M_x: \Delta_Q &\rightarrow -\Delta_{M_x Q} \text{ for } \Delta_Q \in A_u, B_{3u}, \end{aligned} \quad (3)$$

in which $M_x Q$ is the M_x -mirror-transformed wavevector Q . The transformation properties under M_y are

$$\begin{aligned} M_y: \Delta_Q &\rightarrow \Delta_{M_y Q} \text{ for } \Delta_Q \in B_{1u}, B_{3u}, \\ M_y: \Delta_Q &\rightarrow -\Delta_{M_y Q} \text{ for } \Delta_Q \in A_u, B_{2u}. \end{aligned} \quad (4)$$

The transformation properties under M_z are

$$\begin{aligned} M_z: \Delta_Q &\rightarrow \Delta_{M_z Q} \text{ for } \Delta_Q \in B_{2u}, B_{3u}, \\ M_z: \Delta_Q &\rightarrow -\Delta_{M_z Q} \text{ for } \Delta_Q \in A_u, B_{1u}. \end{aligned} \quad (5)$$

The transformation properties of the uniform component, Δ_0 , are related to those above by taking $Q = M_x Q = M_y Q = M_z Q = 0$. If and Δ_Q are surface orders of UTe_2 , their transformation properties can be understood by projecting the bulk irreps onto the surface.

Ginzburg–Landau theory

In this section, we consider a Ginzburg–Landau theory of three triplet PDWs coexisting with uniform triplet superconductivity in a material with D_{2h} symmetry (the same symmetry as UTe_2). As we shall show, this theory leads to daughter CDWs that are suppressed in a magnetic field. Furthermore, when the triplet superconducting orders have finite angular momentum, the suppression is anisotropic, and uneven for different CDWs. This theory is applicable to the situation in which the superconducting, PDW and CDW orders are bulk orders of UTe_2 as well as the situation in which they are surface orders.

The Ginzburg–Landau theory is constructed from a uniform triplet order parameter Δ_0 and triplet PDW order parameters $\Delta_{\pm Q_i}$ with wavevector $\pm Q_i$, and $i = 1, 2, 3$. If we are considering the PDWs to bulk orders, the wavevectors Q_i are defined such that for the cleave surface of the material (defined the same way as in the main text) the wavevectors Q_i project onto q_i^{CDW} . The PDW order parameters therefore project onto surface PDW order parameters of the form $\Delta_{\pm Q_i} \rightarrow \Delta_{\pm q_i^{\text{CDW}}}$ on the cleave surface. If we are instead considering the PDWs to be surface orders, $Q_i = q_i^{\text{CDW}}$.

As M_x mirror symmetry is the only symmetry preserved by the cleave surface, we will primarily consider the transformation properties of the order parameters under M_x . On the cleave surface, mirror symmetry acts as $M_x: q_1^{\text{CDW}} \rightarrow -q_2^{\text{CDW}}$ and $M_x: q_3^{\text{CDW}} \rightarrow -q_3^{\text{CDW}}$. Therefore, $M_x: Q_1 \rightarrow -Q_2$ and $M_x: Q_3 \rightarrow -Q_3$, regardless of whether we are considering surface orders or bulk orders.

The Landau free-energy density for Δ_0 and $\Delta_{\pm Q_i}$ is given by

$$\begin{aligned} \mathcal{F} &= \mathcal{F}_2 + \mathcal{F}_4, \\ \mathcal{F}_2 &= m_0 |\Delta_0|^2 + \sum_i m_i (|\Delta_{Q_i}|^2 + |\Delta_{-Q_i}|^2), \\ \mathcal{F}_4 &= \lambda_{00} |\Delta_0|^4 + \sum_i \lambda_{0i} (|\Delta_{Q_i}|^2 |\Delta_0|^2 + |\Delta_{-Q_i}|^2 |\Delta_0|^2) \\ &\quad + \sum_{ij} \lambda_{ij} (|\Delta_{Q_i}|^2 |\Delta_{Q_j}|^2 + |\Delta_{-Q_i}|^2 |\Delta_{-Q_j}|^2) \\ &\quad + \sum_{ij} \lambda'_{ij} (|\Delta_{Q_i}|^2 |\Delta_{-Q_j}|^2 + |\Delta_{-Q_i}|^2 |\Delta_{Q_j}|^2) \end{aligned} \quad (6)$$

Here $\lambda_{ij} = \lambda_{ji}$, $\lambda'_{ij} = \lambda'_{ji}$. Owing to mirror symmetry, $m_1 = m_2$, $\lambda_{01} = \lambda_{02}$, $\lambda_{11} = \lambda_{12}$ and $\lambda'_{11} = \lambda'_{12}$. For stability, $\lambda_{00}, \lambda_{ii} > 0$. To favour coexistence of the superconducting order parameters, $\lambda_{0i} < 0$ for all i , $\lambda_{ij} < 0$ for $i \neq j$ and $\lambda'_{ij} < 0$ for all i and j . In this section, we are interested only in the values of the order parameters in different phases, and not, for example, in the details of the phase transitions that connect different phases. As a

result, equation (6) can describe either bulk orders (if the Q_i are bulk wavevectors) or surface orders (if the Q_i are surface wavevectors).

In the ordered phase, for which Δ_0 and $\Delta_{\pm Q_i}$ all have expectation values ($m_0, m_i < 0$), there will be daughter CDW orders

$$\begin{aligned}\rho_{Q_i} &\propto \Delta_{Q_i} \cdot \Delta_0^* + \Delta_0 \cdot \Delta_{-Q_i}^*, \\ \rho_{Q_i+Q_j} &\propto \Delta_{Q_i} \cdot \Delta_{-Q_j}^* + a_i \rho_{Q_i} \rho_{Q_j}, \\ \rho_{Q_i-Q_j} &\propto \Delta_{Q_i} \cdot \Delta_{Q_j}^* + b_i \rho_{Q_i} \rho_{-Q_j},\end{aligned}\quad (7)$$

in which a_i and b_i are complex constants, and the CDW order parameters ρ_{Q_i} are a complex scalar field that satisfies $\rho_{Q_i}^* = \rho_{-Q_i}$. If we are considering bulk orders, then on the cleave surface, the CDW operators project onto surface CDW operators $\rho_{Q_i} \rightarrow \rho_{Q_i}^{\text{CDW}}$ and $\rho_{Q_i \pm Q_j} \rightarrow \rho_{Q_i \pm Q_j}^{\text{CDW}}$. If we are considering surface orders, then $Q_i = q_i^{\text{CDW}}$ and $Q_i \pm Q_j = q_i^{\text{CDW}} \pm q_j^{\text{CDW}}$ in equation (7).

In this Landau theory, the daughter orders arise from the following terms

$$\begin{aligned}\mathcal{F}_{\text{CDW}} &= \sum_i m_i^{\text{CDW}} |\rho_{Q_i}|^2 + \sum_{ij} m_{ij}^{\text{CDW}} |\rho_{Q_i+Q_j}|^2 + \sum_{ij} m_{ij}'^{\text{CDW}} |\rho_{Q_i-Q_j}|^2 \\ &+ \sum_i g_{0i} \rho_{Q_i} [\Delta_{Q_i} \cdot \Delta_0^* + \Delta_0 \cdot \Delta_{-Q_i}^*] \\ &+ \sum_{ij} g_{ij} \rho_{Q_i+Q_j} \Delta_{Q_i} \cdot \Delta_{-Q_j}^* + g_{ij}' \rho_{Q_i-Q_j} \Delta_{Q_i} \cdot \Delta_{Q_j}^* \\ &+ \gamma_{ij} \rho_{Q_i+Q_j}^* \rho_{Q_i} \rho_{Q_j} + \gamma_{ij}' \rho_{Q_i-Q_j}^* \rho_{Q_i} \rho_{-Q_j} + \text{h.c.},\end{aligned}\quad (8)$$

in which $m_i^{\text{CDW}}, m_{ij}^{\text{CDW}}, m_{ij}'^{\text{CDW}} > 0$. On this basis, when Δ_{Q_i} and Δ_0 are non-zero, the free energy is minimized when the CDWs are also non-zero. For brevity, we have omitted the quartic terms from \mathcal{F}_{CDW} , although such terms are allowed by symmetry. We should note that if one considers the case of a system with CDW and uniform superconducting coexistent orders, then a modulated ('PDW') component would be induced by the first of the cubic terms. Thus, the Landau theory does not distinguish these two scenarios. This will be discussed in more detail towards the end of this section.

We now add an external magnetic field \mathbf{H} to the Landau theory. If we include a gradient term in the free-energy expansion, the magnetic field minimally couples to the superconducting orders as $|D_\mu \Delta_0|^2$, and $|D_\mu \Delta_{\pm Q_i}|^2$, in which $D_\mu = \partial_\mu - i2eA_\mu$, A_μ is the electromagnetic gauge field and μ labels the space-time coordinates. As the superconducting orders are spin-triplet orders, they can have a finite angular momentum that also couples to the magnetic field. The angular momenta of the superconducting orders are $i\Delta_0 \times \Delta_0^*$ and $i\Delta_{\pm Q_i} \times \Delta_{\pm Q_i}^*$, and they couple to the external magnetic field through

$$\mathcal{F}_{\text{Mag}} = -\epsilon_0 \mathbf{H} \cdot (i\Delta_0 \times \Delta_0^*) - \sum_j \epsilon_j \mathbf{H} \cdot (i\Delta_{Q_j} \times \Delta_{Q_j}^*) - \sum_j \epsilon_j' \mathbf{H} \cdot (i\Delta_{-Q_j} \times \Delta_{-Q_j}^*) \quad (9)$$

Here $\epsilon_0, \epsilon_j > 0$ and mirror symmetry requires that $\epsilon_1 = \epsilon_2$. For time-reversal-invariant systems, the angular momenta all vanish^{1,10}. However, if time-reversal symmetry is broken, the angular momentum can be non-vanishing, $(i\Delta_0 \times \Delta_0^*) \neq 0, (i\Delta_{\pm Q_i} \times \Delta_{\pm Q_i}^*) \neq 0$. As $\epsilon_0, \epsilon_j > 0$, it is energetically favourable for the angular momentum to aligned with the magnetic field. Here, non-vanishing angular momentum also requires the order parameters to be sums of different irreps (for bulk orders) or sums of different surface-projected irreps (for surface orders)¹⁰. When the superconducting order parameters are combinations of different irreps, each irrep should correspond to a distinct term in the Ginzburg-Landau theory. Nevertheless, for simplicity, we have assumed that the Ginzburg-Landau theory can be written in terms of the superconducting orders Δ_{Q_i} and Δ_0 , instead of the distinct irreps. This simplification does not reflect the fact that different irreps will, in general, transition at different temperatures. However, as we are interested in physics that is far away from any transitions, this

additional feature does not change the qualitative features of our analysis.

Owing to the minimal coupling between the superconducting orders and A_μ , the superconducting orders are suppressed in an external magnetic field, and above an upper critical field the superconducting orders (and by extension the daughter CDW orders) will vanish. The Ginzburg-Landau theory therefore correctly predicts the suppression of the CDW orders in an external magnetic field. Owing to the coupling between the angular momentum and magnetic field, the upper critical field will be higher when the magnetic field is aligned with the angular momentum of a superconducting order and lower when they are anti-aligned.

If M_x mirror symmetry is preserved by the $\Delta_{\pm Q_1}$ and $\Delta_{\pm Q_2}$ PDWs, their respective angular momenta are related through

$$\begin{aligned}\hat{y} \cdot \langle i\Delta_{\pm Q_1} \times \Delta_{\pm Q_1}^* \rangle &= -\hat{y} \cdot \langle i\Delta_{\mp Q_2} \times \Delta_{\mp Q_2}^* \rangle, \\ \hat{z} \cdot \langle i\Delta_{\pm Q_1} \times \Delta_{\pm Q_1}^* \rangle &= -\hat{z} \cdot \langle i\Delta_{\mp Q_2} \times \Delta_{\mp Q_2}^* \rangle,\end{aligned}\quad (10)$$

In this case, for $H_y \neq 0$, or $H_z \neq 0$, the $\Delta_{\pm Q_1}$ PDW will be more suppressed than the $\Delta_{\pm Q_2}$ PDW or vice versa. Which of the two is more suppressed depends on the sign and magnitude of H_y and H_z . This agrees with the observed mirror-symmetry breaking.

We note that the Ginzburg-Landau theory predicts existence of both ρ_{Q_i} and $\rho_{Q_i \pm Q_j}$ daughter CDWs. Both types of CDW are observed in UTe_2 , but the $\rho_{Q_i \pm Q_j}$ CDWs are weaker than the ρ_{Q_i} CDWs. A possible explanation for this is that the amplitudes of the PDW order parameters are weaker than that of the uniform superconducting order parameter

$$|\langle \Delta_{\pm Q_i} \rangle| \ll |\langle \Delta_0 \rangle| \quad (11)$$

In this case, the ρ_{Q_i} CDWs would be the dominant charge orders, as ρ_{Q_i} is linear in the PDW order parameters, whereas $\rho_{Q_i \pm Q_j}$ is quadratic in PDWs.

The Ginzburg-Landau theory presented here can also be adapted to describe the situation in which the uniform superconductivity and CDWs are primary orders and the PDWs occur as daughter orders. To do this, let us first assume that the PDWs are not primary orders (that is, the PDW masses m_i are positive). We also need to include the following quartic CDW terms

$$\mathcal{F}_{\text{CDW}}^4 = \sum_i \lambda_i^{\text{CDW}} |\rho_{Q_i}|^4 + \dots, \quad (12)$$

in which ... indicates various bi-quadratic terms between different CDW orders and the superconducting and PDW orders. We take the bi-quadratic terms to be tuned such that they favour coexistence of the uniform superconductivity and CDW orders. When $m_i^{\text{CDW}} < 0$ and $\lambda_i^{\text{CDW}} > 0$, the CDW order parameter ρ_{Q_i} acquires a non-vanishing expectation value. If the uniform superconductivity Δ_0 coexists with the CDWs, the PDW order parameters $\Delta_{\pm Q_i}$ will acquire expectation values because of the tri-linear terms in equation (8). This leads to the correct intertwined orders. However, this scenario does not explain why the CDWs are suppressed in an external magnetic field, as the charge-neutral CDW order parameters do not minimally couple to A_μ .

Melting the PDWs and uniform superconductivity

Finally, we briefly discuss the potential role of vortices in the destruction of the PDWs and the uniform superconductivity. Let us consider the situation in which the PDWs and the uniform superconductivity host random vortices of the form

$$\begin{aligned}\Delta_0 &\rightarrow e^{i\theta_v} \Delta_0, \\ \Delta_{\pm Q_i}^{\text{CDW}} &\rightarrow e^{i\theta_v} \Delta_{\pm Q_i}^{\text{CDW}},\end{aligned}\quad (13)$$

in which θ_v is a U(1) phase that winds by a multiple of 2π around the vortices⁴⁴. Here all of the PDWs and the uniform superconductivity share the same vortices. When these vortices proliferate, the expectation values of the PDWs and the uniform superconductivity all vanish.

Article

However, the vortex proliferation does not cause the expectation values of the CDWs to vanish, as $\rho_{q_{\text{CDW}}}$ does not depend on the vortex phase θ_v (see equation (7)). As such, proliferation of the vortex in equation (13) leads to a phase in which the daughter CDW orders persist in the absence of the parent PDW and uniform superconducting orders. It is not clear at this stage whether this vortex proliferation accurately describes the destruction of superconductivity at T_c and the observation of CDWs at 4 K. However, our arguments do indicate that the observation of CDWs at 4 K is not inconsistent with the PDW scenario we have presented in this work.

Data availability

All of the data for the main figures have been uploaded to the Illinois Databank (https://doi.org/10.13012/B2IDB-1713879_V1).

43. Gelessus, A., Thiel, W. & Weber, W. Multipoles and symmetry. *J. Chem. Educ.* **72**, 505–508 (1995).
44. Berg, E., Fradkin, E. & Kivelson, S. Charge-4e superconductivity from pair-density-wave order in certain high-temperature superconductors. *Nat. Phys.* **5**, 830–833 (2009).

Acknowledgements We thank S.Kivelson and Q.Si for useful discussions. STM studies at the University of Illinois, Urbana-Champaign were supported by the US Department of Energy,

Office of Science, Office of Basic Energy Sciences, Materials Sciences and Engineering Division under award number DE-SC0022101. V.M. acknowledges partial support from Gordon and Betty Moore Foundation's EPIQS Initiative through grant GBMF4860 and the Quantum Materials Program at CIFAR where she is a Fellow. Theoretical work was supported in part by the US National Science Foundation through the grant DMR 1725401 and DMR 2225920 at the University of Illinois (E.F. and L.N.) and by a postdoctoral fellowship of the Institute for Condensed Matter Theory of the University of Illinois (L.N.). J.M.-M. acknowledges support by ARO MURI grant number W911NF2020166. Research at the University of Maryland was supported by the Department of Energy award number DE-SC-0019154 (sample characterization), the Gordon and Betty Moore Foundation's EPIQS Initiative through grant number GBMF9071 (materials synthesis), the National Science Foundation under grant number DMR-2105191 (sample preparation), the Maryland Quantum Materials Center and the National Institute of Standards and Technology. S.R.S. acknowledges support from the National Institute of Standards and Technology Cooperative Agreement 70NANB17H301.

Author contributions A.A. and V.M. conceived the experiments. The single crystals were provided by S.R., S.R.S., J.P. and N.P.B. M.R. carried out the Laue characterization of the single crystals. A.A. and A.R. obtained the STM data. A.A. and V.M. carried out the analysis and J.M.-M., L.N. and E.F. provided the theoretical input on the interpretation of the data. A.A., V.M., J.M.-M. and E.F. wrote the paper with input from all authors.

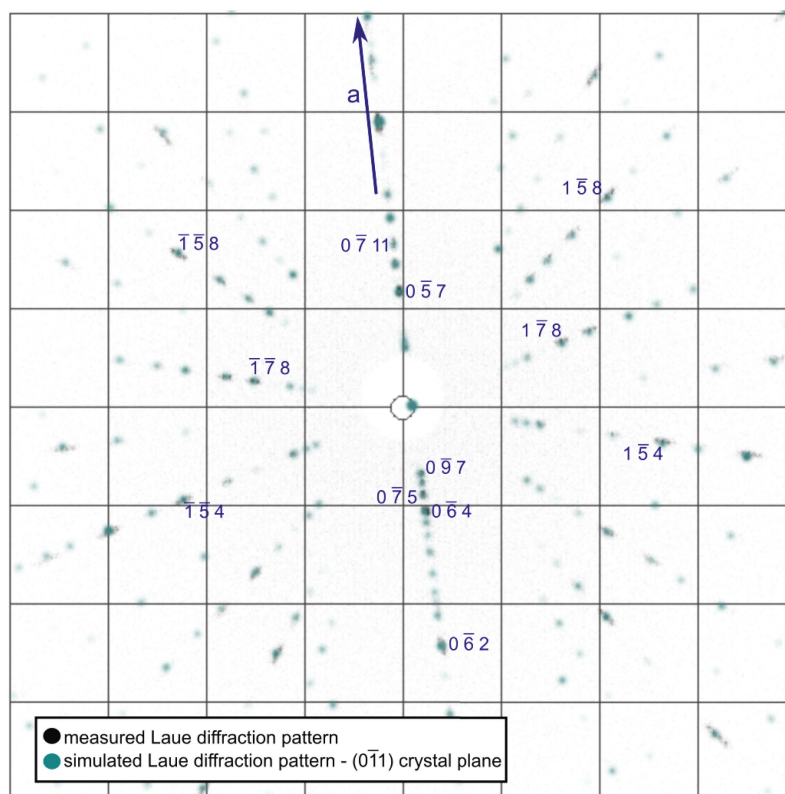
Competing interests The authors declare no competing interests.

Additional information

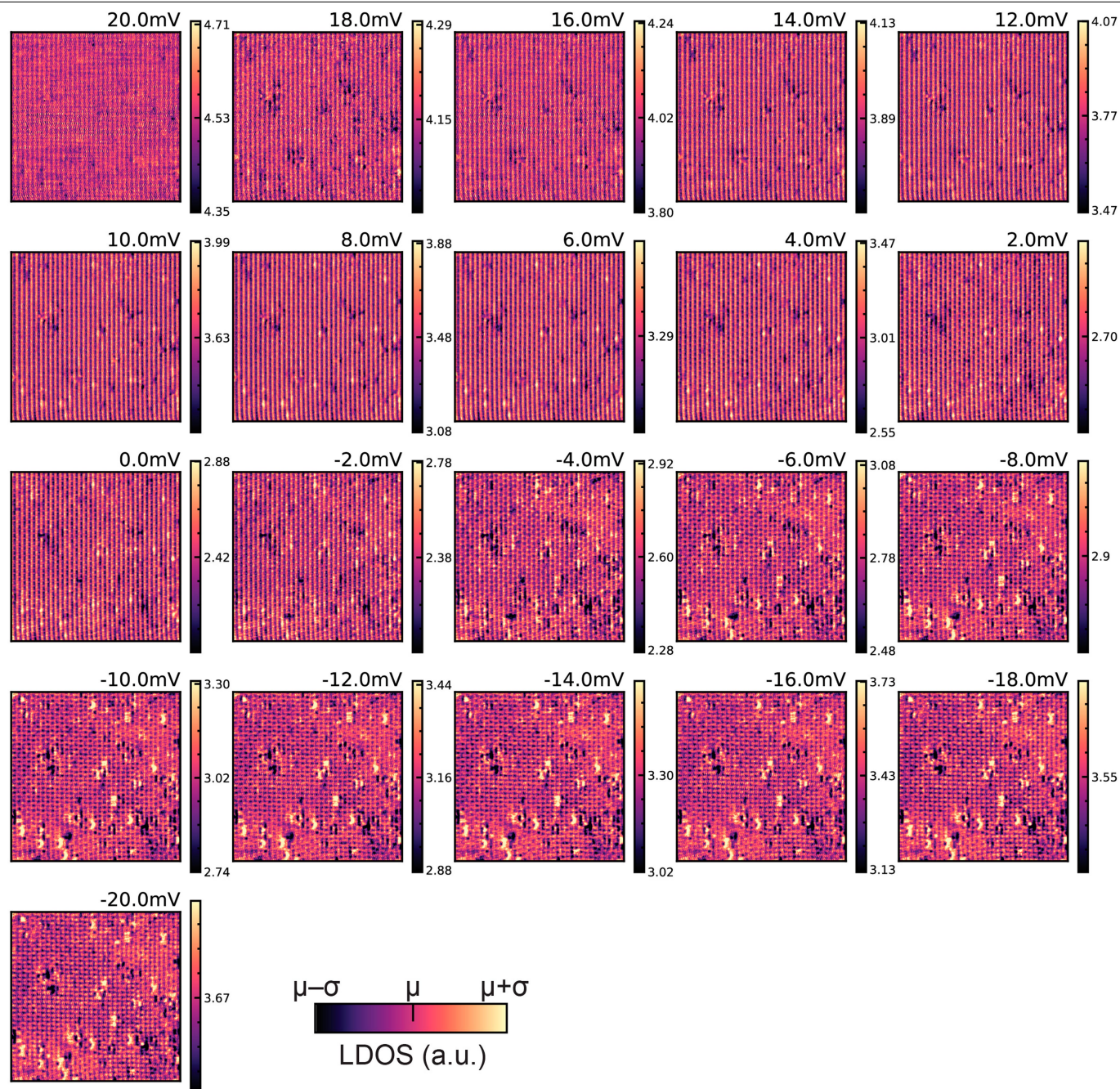
Correspondence and requests for materials should be addressed to Vidya Madhavan.

Peer review information *Nature* thanks the anonymous reviewers for their contribution to the peer review of this work.

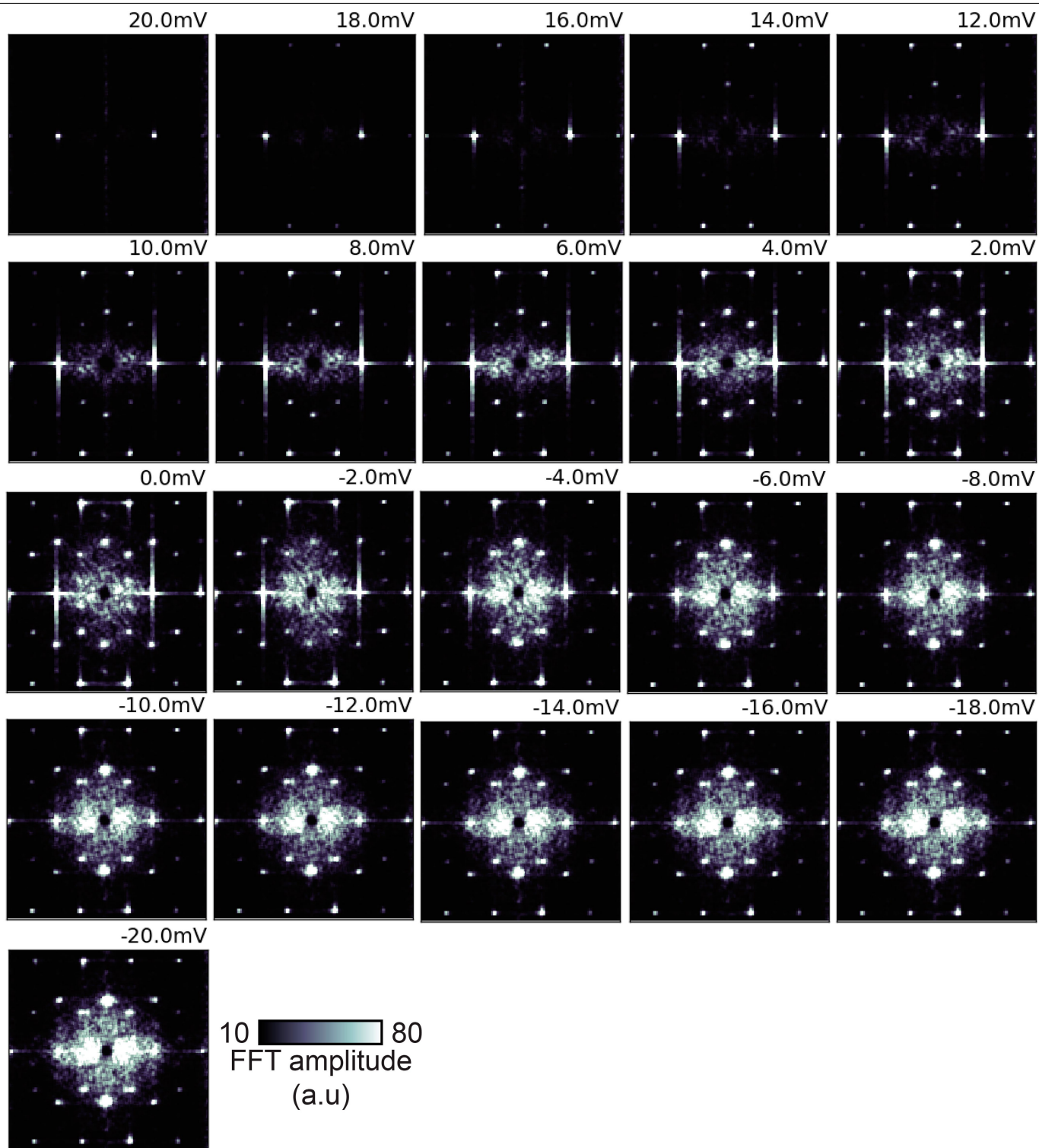
Reprints and permissions information is available at <http://www.nature.com/reprints>.



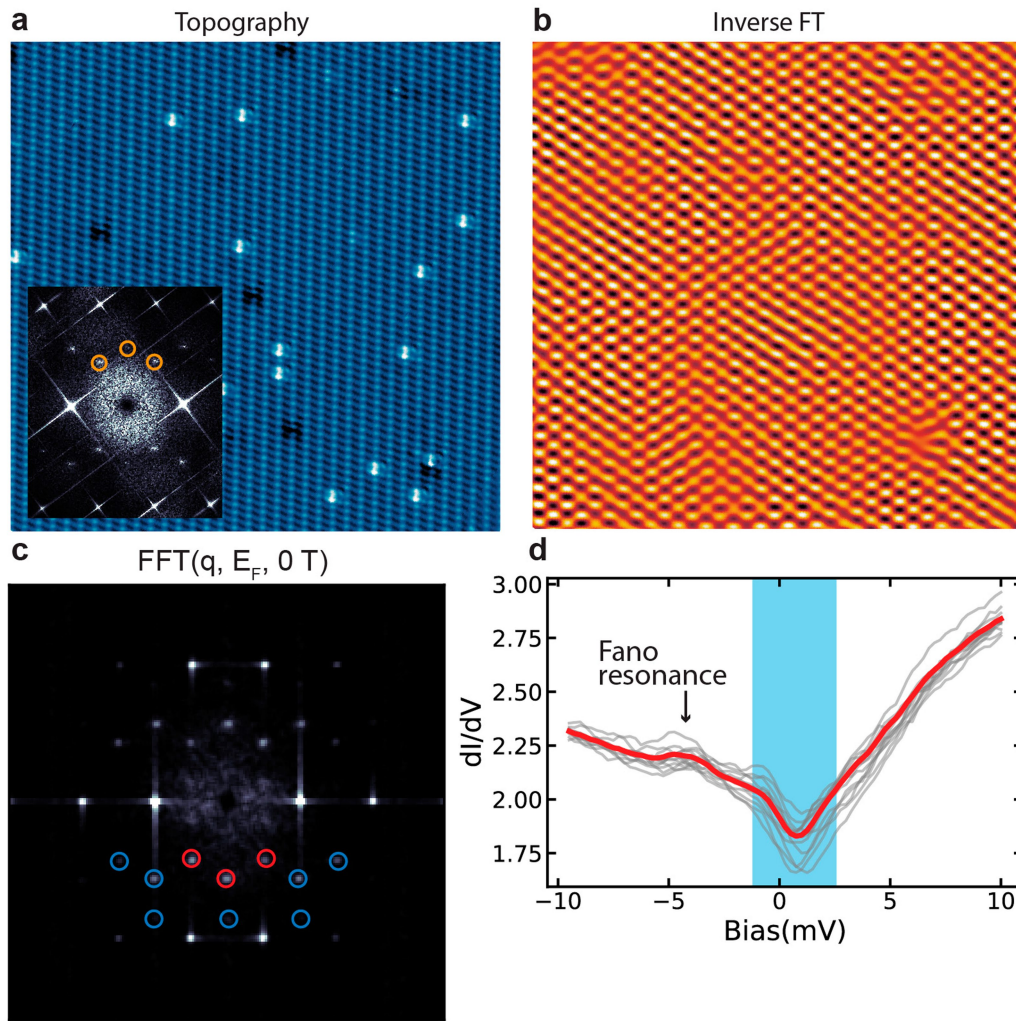
Extended Data Fig. 1 | Laue diffraction from the (011) aligned crystal. Laue diffraction of a single UTe_2 crystal which was used for the STM study is shown. A few specific (hkl) surfaces are marked.



Extended Data Fig. 2 | LDOS at 300 mK. LDOS maps obtained at several energies above and below E_F .

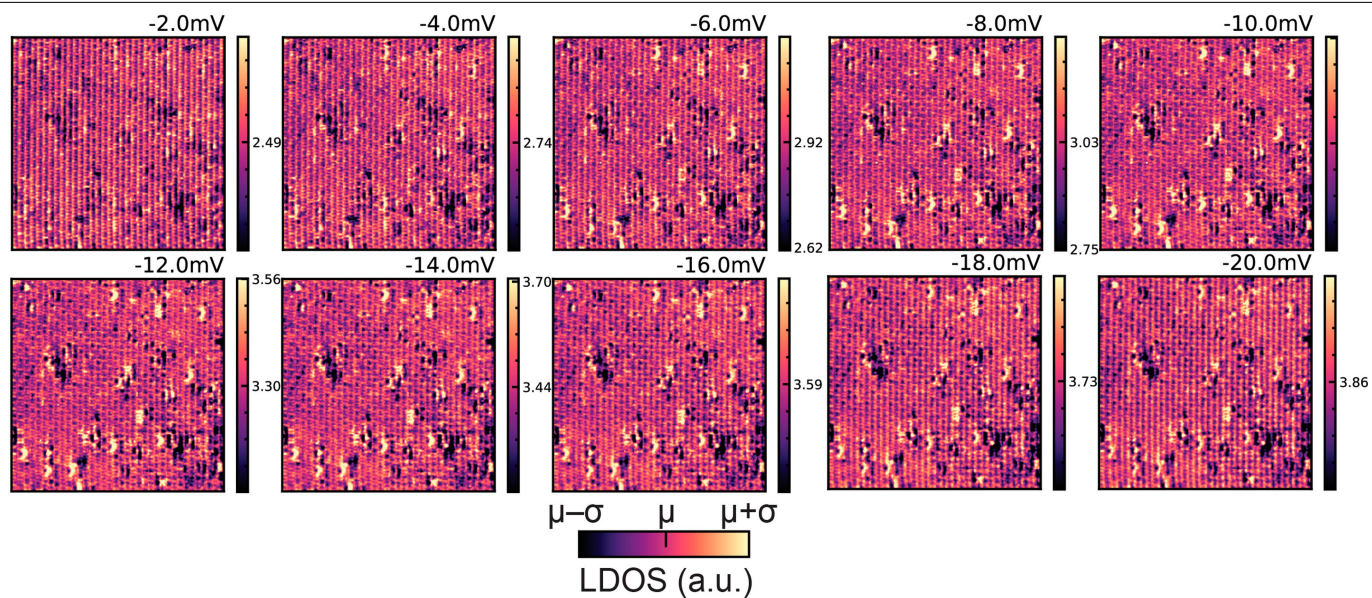


Extended Data Fig. 3 | FFT of LDOS at 300 mK. FFTs of LDOS maps obtained at several energies above and below E_F .

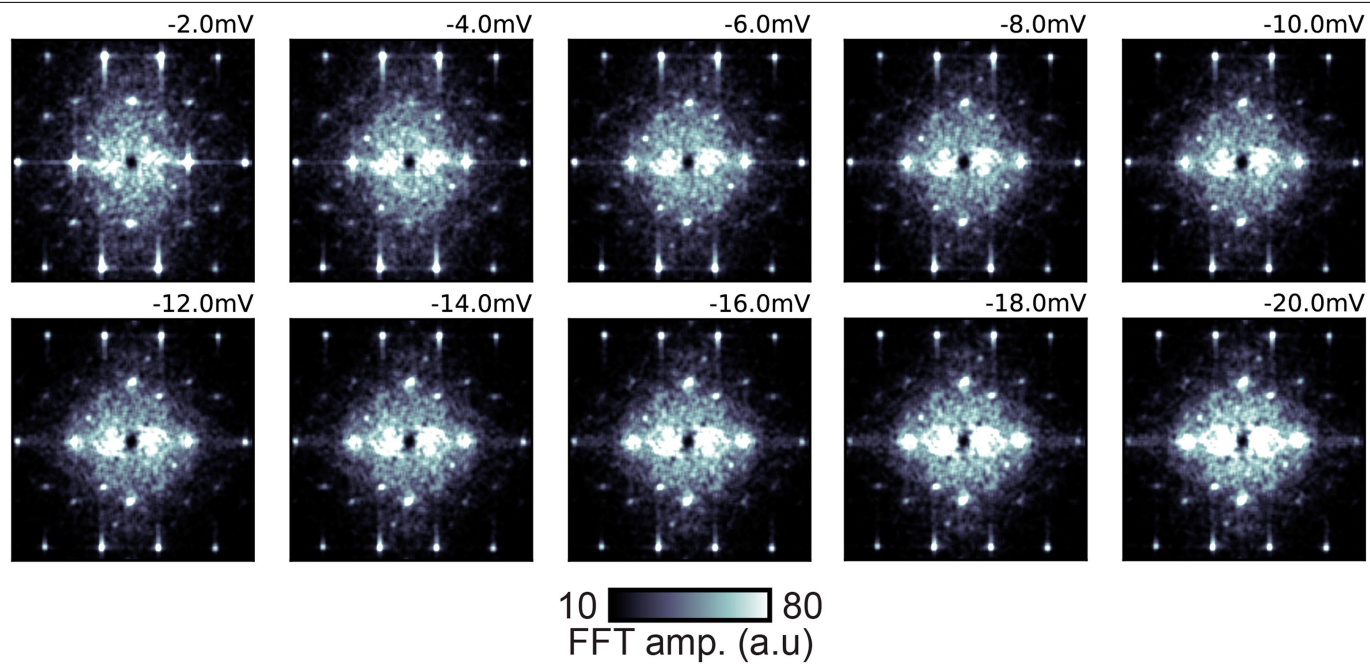


Extended Data Fig. 4 | Inverse FFT of the CDW peaks, FFT showing primary and secondary CDW peaks and low energy dI/dV spectra. **a,** Topography obtained on the (011) surface (same area as that shown in Fig. 1c of the manuscript. Inset shows the corresponding FFT with the CDW peaks circled in orange. **b**, Inverse FFT obtained from the circled CDW peaks (in orange) allowing real space visualization of the CDW modulations. **c**, FFT at the E_F where

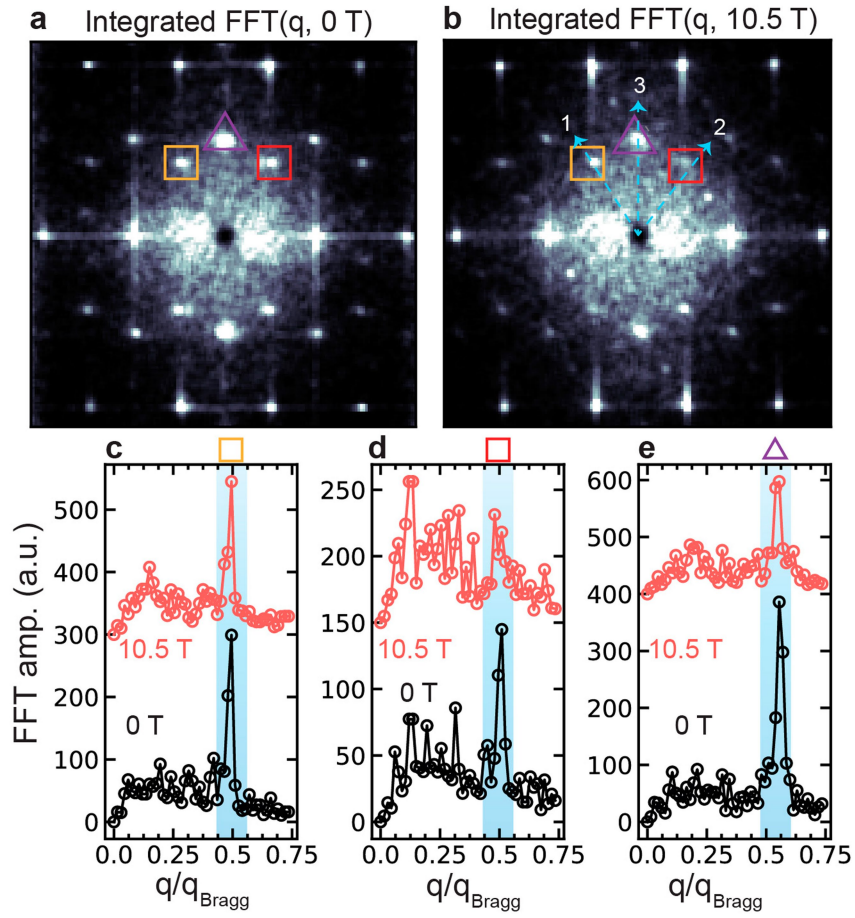
the primary and secondary CDWs are shown using red circles and blue circles respectively, **d**, Linecut of the dI/dV spectra (shown in grey) and the average dI/dV spectrum (shown in red) obtained along the Te-chains. Apart from the Fano lineshape associated with the Kondo resonance, the individual spectra and the average dI/dV spectrum show an additional low energy feature (slope change around -1 meV to $+2$ meV) shown by the blue shaded region.



Extended Data Fig. 5 | LDOS in presence of a 10.5 T magnetic field. LDOS maps obtained at several energies in a perpendicular magnetic field.



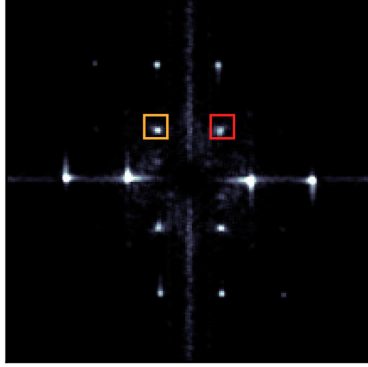
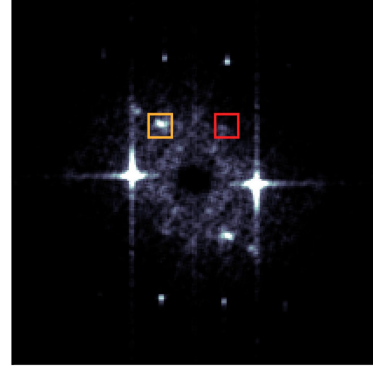
Extended Data Fig. 6 | FFT of LDOS in presence of a 10.5 T magnetic field. FFTs of LDOS maps obtained at several energies in a perpendicular magnetic field.




Extended Data Fig. 7 | Partial suppression and mirror symmetry breaking of the CDWs in the integrated FFT signal. **a-b**, Comparison of FFTs of integrated signal obtained from integrating LDOS maps below E_f for a 0 T field and 10.5 T field. The FFT of the integrated signal also shows similar behavior as

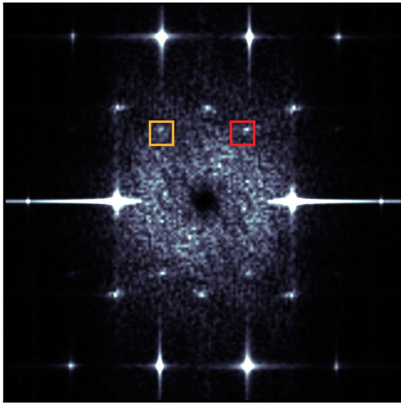
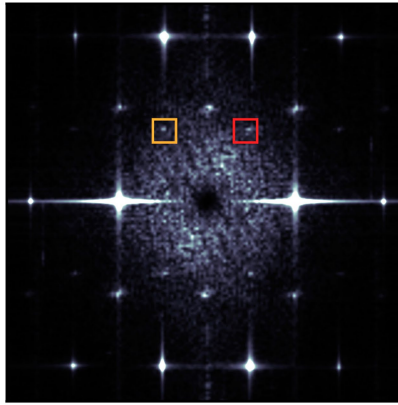
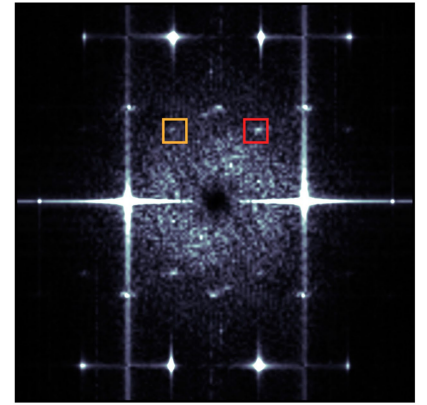
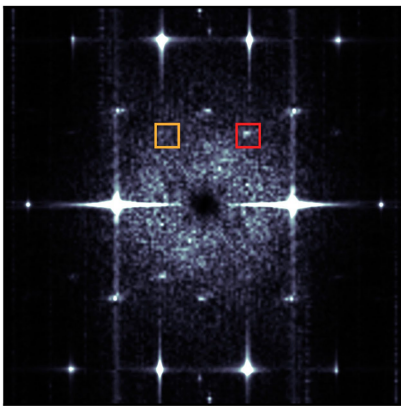
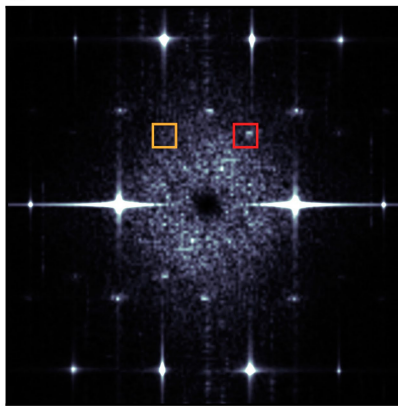
the FFT of individual energy slices. **c-e**, Linecuts obtained along 3 different directions for the 3 CDWs illustrating the mirror symmetry breaking. **d** is clearly more suppressed than **c**.

Dataset 2 with second sample-tip combination

a FFT(q , -10 meV, 0 T)**b** FFT(q , -10 meV, 10.5 T)

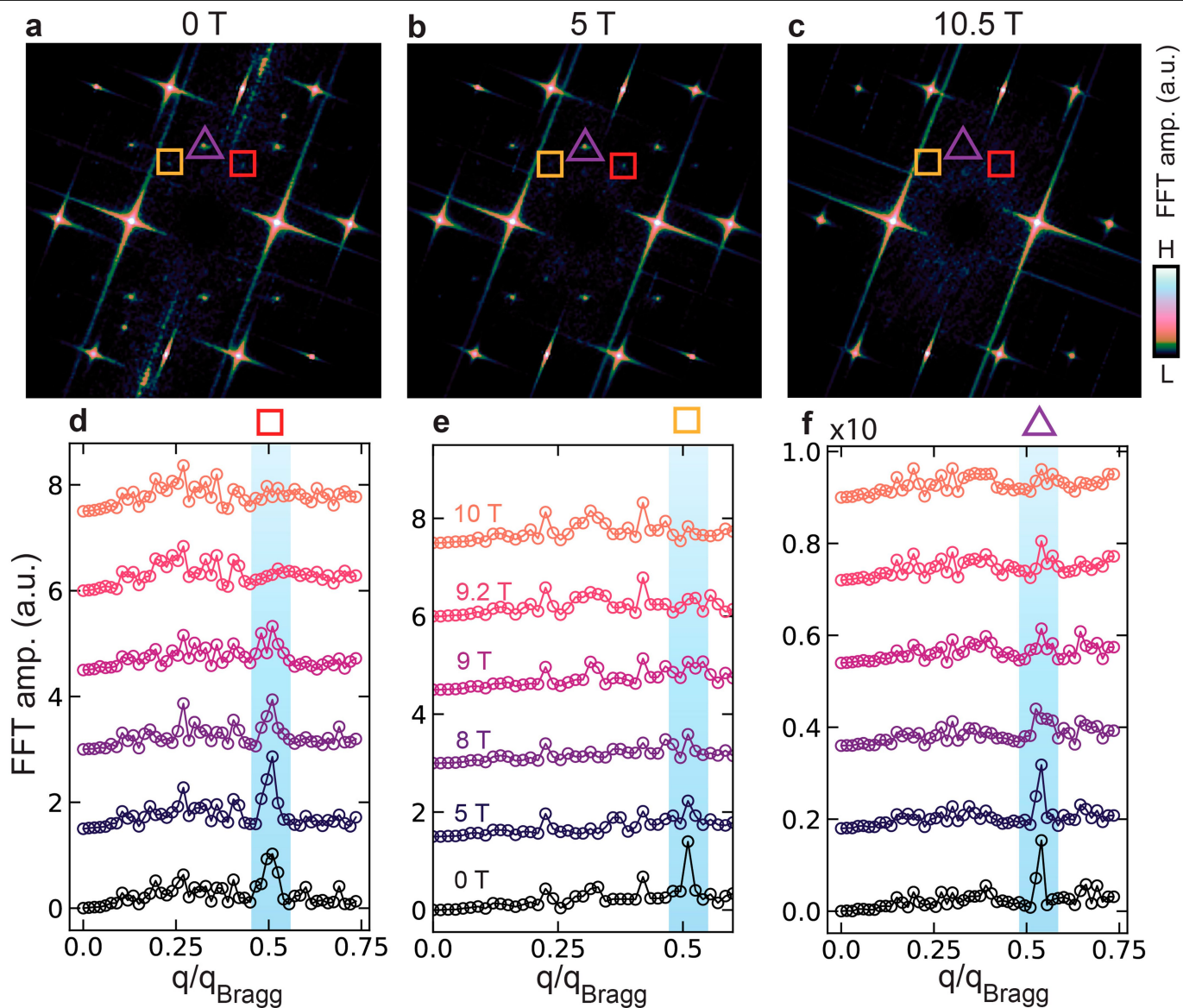
L  H
FFT amp. (a.u.)

Dataset 3 with third sample-tip combination

c 5 T**d** 7 T**e** 8 T**f** 10 T**g** 11 T

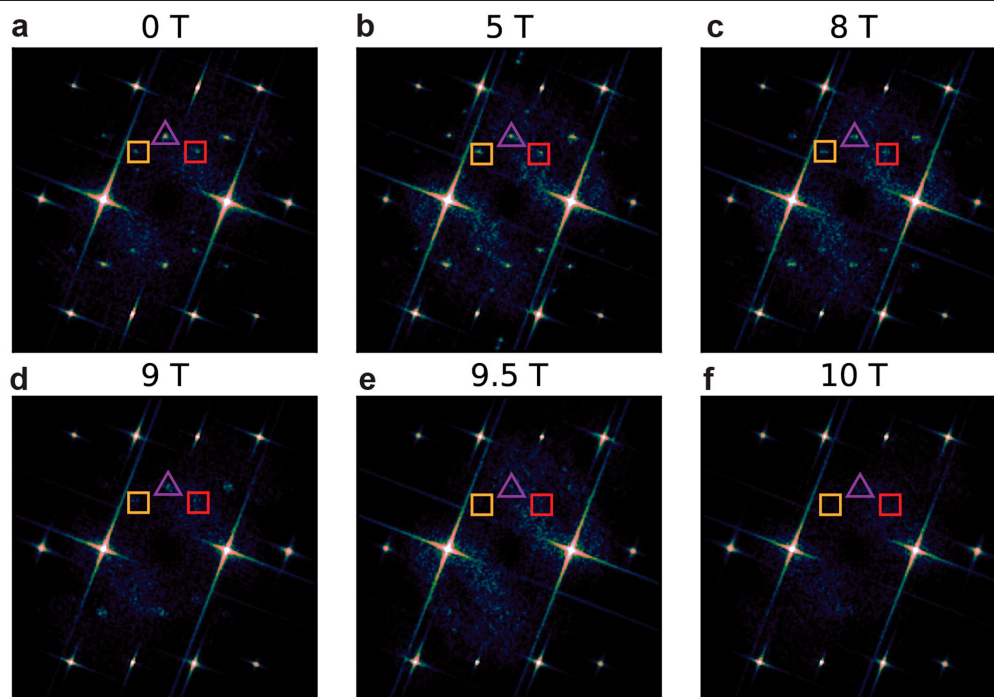
Extended Data Fig. 8 | Second and third sample-tip combinations for perpendicular magnetic field showing reproducibility of the partial suppression and mirror symmetry breaking of the CDW at 10.5 T. **a–b**, Second dataset obtained with a different tip-sample combination showing the partial suppression and mirror symmetry breaking of the CDW in a perpendicular

magnetic field. The FFTs shown have the same intensity scale. **c–g**, Series of FFTs of topographies as a function of increasing magnetic field perpendicular to the [011] surface with a third sample-tip combination. ($V = 20$ mV, $I = 100$ pA) The intensity scale of all FFTs has been kept constant. The critical field for the mirror-symmetry breaking in q_1^{CDW} and q_2^{CDW} is close to 10 T.



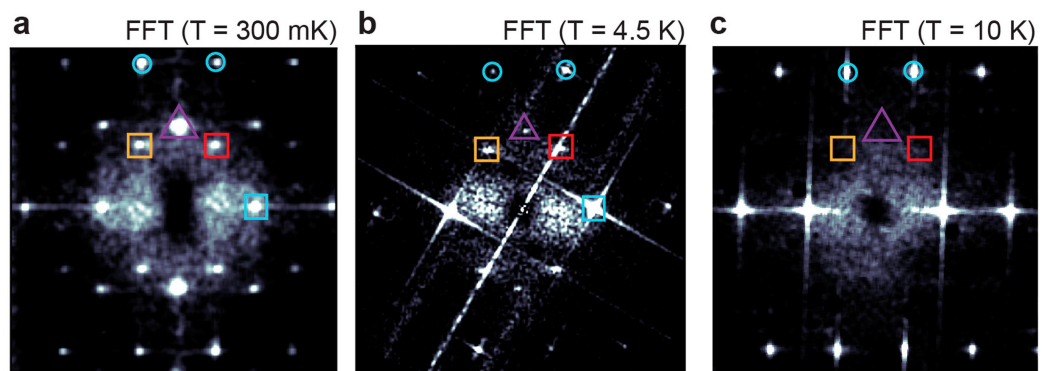
Extended Data Fig. 9 | FFTs showing the suppression of the CDWs at positive bias in a 11-degree tilted magnetic field. **a–c**, Series of FFT of topographies obtained as a function of increasing magnetic field at 11 degrees with respect to the [011] direction with a different tip. ($V = 40$ mV, $I = 120$ pA). The intensity

scale of all FFTs has been kept constant. The surface tilt is measured using the tilt correction function in the Nanonis module. **d–f**, Fourier transform linecuts obtained along 3 different directions of the CDWs as a function of magnetic field, showing clear suppression of the peak amplitudes above 9 T.



Extended Data Fig. 10 | Additional dataset with a different tip showing reproducibility of the suppression of the CDWs in a 11-degree tilted magnetic field. a–f, Additional dataset showing a series of FFT of topographies obtained as a function of increasing magnetic field at 11 degrees with respect to

the [011] direction with a different tip. ($V = 50$ mV, $I = 150$ pA). The intensity scale of all FFTs has been kept constant. The surface tilt is measured using the tilt correction function in the Nanonis module.



Extended Data Fig. 11 | Melting of the CDWs as a function of temperature. a–c, FFTs of LDOS maps obtained as a function of temperature. The CDWs persist till 4 K and have disappeared by 10 K.